DOI: 10.48011/sbse.v1i1.2490

OPF-based Active Network Management Strategy for Distribution Networks with High Penetration of Distributed Generation

Celso Rocha * **Paulo Radatz** ** **Carlos Almeida** *** **Nelson Kagan** ****

* *Departamento de Engenharia de Energia e Automação Elétricas da Escola Politécnica da Universidade de São Paulo, SP, (e-mail: celso.rocha@usp.br).*
** *Departamento de Engenharia de Energia e Automação Elétricas da Escola Politécnica da Universidade de São Paulo, SP, (e-mail: paulo.radatz@usp.br).*
*** *Departamento de Engenharia de Energia e Automação Elétricas da Escola Politécnica da Universidade de São Paulo, SP, (e-mail: cfmalmeida@usp.br).*
**** *Departamento de Engenharia de Energia e Automação Elétricas da Escola Politécnica da Universidade de São Paulo, SP, (e-mail: nelsonk@pea.usp.br).*

Abstract: This paper presents a near real-time strategy for Active Network Management (ANM) considering distribution networks with high penetration of Distributed Generation (DG). It is built upon a centralized framework and availability of a broad communication infrastructure. Generation curtailment level of Medium Voltage (MV), residential and commercial-scale Photovoltaic (PV) systems are considered as control variables to manage voltage and asset loading levels in MV and Low-Voltage (LV) distribution networks through a three-phase unbalanced Non-Linear (NL) Optimum Power Flow (OPF) algorithm. The effectiveness of the strategy in maintaining the regulatory operational levels, its robustness and the effect of the processing and communication delays are assessed by simulating a real Brazilian network with 788 control elements.

Keywords: Active Network Management; Distributed Generation; Optimum Power Flow; Generation Curtailment; Power Quality; Distribution Operation.

1. INTRODUCTION

The connection of DG has massively been increasing in the world boosted by economical, regulatory, technological and socioenvironmental factors, with emphasis to the photovoltaic renewable generation whose global installed capacity surpassed 200 GW in 2018 (around 40% of the total PV installed capacity). Forecasting studies also indicated that installed capacity will reach about 530 GW in the next five years (International Energy Agency (IEA), 2019). In the Brazilian context, the distributed PV installed capacity grows exponentially and has reached 1.72 GW in 2019 from which 66% were added in the same year and 79% are equally distributed between residential and commercial LV Consumer Units (CU) (ANEEL, 2019).

High variable DG penetration levels impose challenges to the operation of distribution systems, particularly in LV networks, where traditionally there is low monitoring and control. Specially in these networks, the traditional technique to secure adequate levels of voltage and assets' loading at the planning stage by considering extreme conditions of maximum generation and minimum demand tends to substantially limit the practical DG installed capacity.

Corroborated by recent international (IEEE, 2018) (Bruendlinger, 2016) and national (ABNT, 2013) standards as well as flexible interconnection agreements, different ANM strategies have been proposed in the last 15 years. For instance, the utilization of local control systems based on smart inverter functions with voltage regulation capabilities (Seal and Ealey, 2016), for the specific case of voltage violations mitigation, or yet, more sophisticated solutions, such as autonomous systems responsible for monitoring selected lines segments and executing generation curtailment as soon as either voltage or loading violations are detected based on pre-established rules (Currie et al., 2007).

Although such strategies are cost-effective from the deployment perspective as they require few or no extra equipment from the Distribution Network Operator (DNO), making them well-suited for low-to-middle penetration levels, they do not effectively use all flexibility provided by the available resources - not only DG, but also other Distributed Energy Resources (DER). For this reason, these solutions are seen as an intermediate step towards a complete DER

integration to the network operation. However, networks with high penetration of DER need more advanced control techniques, which should be able to mitigate violations of multiples operational aspects, to utilize all control elements available and, at the same, to harvest the maximum amount of renewable energy as possible.

The Advanced Distribution Management System (ADMS) is an entity able to integrate all these features to the grid operation in real-time, optimizing their use in a coordinated and centralized manner (Argonne National Laboratory, 2015b). On the one hand, integrating these resources one gains flexibility to realize the full potential of the DER, on the other hand, complexity is added due to the amount of solutions that can be adopted and control elements to be managed simultaneously. The utilization of classical OPF methods pose as a technically feasible solution to holistically mitigate voltage and loading violation issues while seeking to minimize the generation curtailment.

This paper utilizes OPF as a tool for a near real-time ANM strategy with centralized control architecture aiming to mitigate voltage and loading violations in high PV penetration MV and LV feeders while minimizing the generation curtailment. It builds upon modern distribution systems, with the availability of metering infrastructure that allows the necessary visibility to estimate the network state. Thus, a realistic modeling of the communication delays and grid topology is considered.

In section 2, the centralized framework is presented. In section 3, the NL OPF for curtailment minimization is formulated. In section 4, the implementation of the centralized framework in a simulation environment is shown. In section 5, the network under study is detailed and, next, the results of the application of the proposed strategy are presented and analyzed. In section 6, comments regarding practical implementation aspects are made and the conclusions are drawn.

2. CENTRALIZED FRAMEWORK

Figure 1 conceptually shows some of the corporate systems presently utilized by DNO and involved in the ANM strategy adopted. The calculation engine corresponds to an autonomous application implemented in the ADMS, however the communication with other systems plays an important role. For instance, the connection data of the several equipment that comprise the grid, stored in the Geographic Information System (GIS), are utilized along with the state of the substation and field switches in the execution of the topology processor (Argonne National Laboratory, 2015a), an ADMS application responsible for determining the bus-line model of the network, which is further used by other applications. The Distribution System State Estimation (DSSE) is one of those applications. It estimates the voltage levels of all nodes of the network, allowing, for instance, violations to be detected even in not directly monitored portions of the grid. Recent fast implementations of DSSE can have execution times as fast as a few seconds (Hrnjic et al., 2017), sufficient for the near-real time operation of the ANM strategy proposed in this work. Another important corporate system that plays a fundamental role in the framework assumed in this work is the *Advanced Metering System* (AMI) which allows

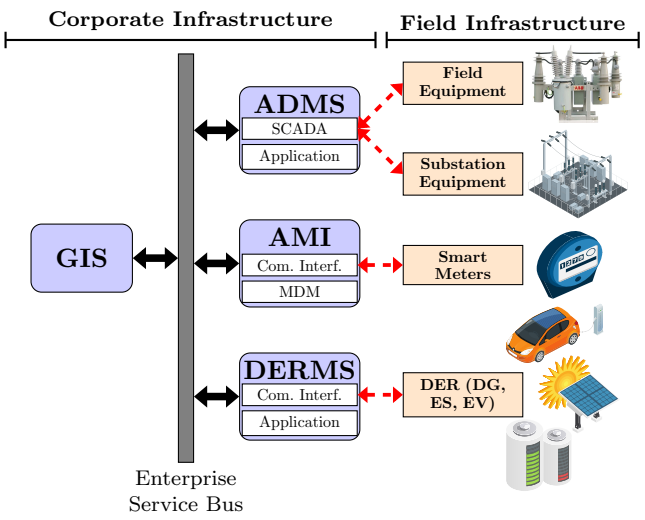

Figure 1. Centralized framework concept.

data such as active power, reactive power and voltages at each CU to be sent to the control room in near real-time or to access historical data stored in Meter Data Management (MDM) systems, in case the near real-time data is not available.

Finally, regarding the DER (DG, Energy Storage (ES), Electric Vehicles (EV)), the system responsible to integrate them to the network operation for monitoring and control is the Distributed Energy Resources Management System (DERMS). This system is able to gather demand and generation measurements in real-time and to send curtailment levels commands to each generation unit under control, among several other functionalities (Seal et al., 2018).

3. MATHEMATICAL FORMULATION

The mathematical formulation utilized in this work is NL, non-convex and with continuous variables. The state variables are the powers injected in each element of the network, the angle and the magnitude of the nodal voltages, as shown below:

a. Objective Function:
The objective function corresponds to the minimization of the generation curtailment, however, in an equivalent manner, the maximization of the power available by the solar resource has been adopted.

$$maximize \sum_{g \in G} \sum_{\phi \in \Phi} P_{\phi}^{g} + \sum_{g_{\delta} \in G_{\delta}} \sum_{\phi \in \Phi} P_{\phi}^{g_{\delta}} \qquad (1)$$

where P_{ϕ}^{g} is the power generated by a single or three-phase PV generator, g (set G), in each phase ϕ (set Φ) and $P_{\phi}^{g_{\delta}}$ is the power generated by a two-phase generator, g_{δ} (setG_{δ}). This distinction between generators (and also loads, as shown later in the power balance equations) is due to the fact that the actual power generated in each phase for two-phase elements depend on the voltages of the nodes to which each element is connected to. This relation is expressed in appendix A.

b. Power Balance:

Equations (2) and (3) represent Kirchhoff's current law in terms of active and reactive power, respectively, and are responsible for ensuring their balance.

$$\sum_{s\in S|\beta^s=n} P^s_\phi + \sum_{g\in G|\beta^g=n} P^g_\phi + \sum_{g_\delta\in G_\delta|\beta^{g_\delta}=n} P^{g_\delta}_\phi = P_{n,\phi} + \sum_{u_\delta\in U_\delta|\beta^{u_\delta}=n} P^{u_\delta}_\phi + \sum_{l\in L|\beta^l_{①}=n} P^l_{①,\phi} + \sum_{l\in L|\beta^l_{②}=n} P^l_{②,\phi} + \sum_{t\in T|\beta^t_{①}=n} P^t_{①,\phi} + \sum_{t\in T|\beta^t_{②}=n} P^t_{②,\phi} \quad \forall n\in N, \phi\in\Phi \tag{2}$$

$$\sum_{s\in S|\beta^s=n} Q^s_\phi + \sum_{c\in C|\beta^c=n} Q^c_\phi = Q_{n,\phi} + \sum_{u_\delta\in U_\delta|\beta^{u_\delta}=n} Q^{u_\delta}_\phi + \sum_{l\in L|\beta^l_{①}=n} Q^l_{①,\phi} + \sum_{l\in L|\beta^l_{②}=n} Q^l_{②,\phi} + \sum_{t\in T|\beta^t_{①}=n} Q^t_{①,\phi} + \sum_{t\in T|\beta^t_{②}=n} Q^t_{②,\phi} \quad \forall n\in N, \phi\in\Phi \tag{3}$$

where the first term of each equation corresponds to the summation of the powers injected into the node defined by bus n (set N) and phase ϕ; the second term correspond to the summation of the power that leave the node (n, ϕ); $P_{n,\phi}$ and $Q_{n,\phi}$ are the active and reactive power demanded by node (n, ϕ); s represents a network supply element (set S); u_δ represents a two-phase CU element (set U_δ); l represents a line segment (set L); t represents a transformer element (set T); c represents a capacitor element (set C); ① and ② represent the terminals of line and transformer elements; β is a parameter that maps the bus n to which each element u_δ, g, g_δ or c or terminal of a line or transformer element is connected.

c. Power Injected Into Two-Terminal Elements:

The active and reactive powers injected into each phase of each terminal of lines, l, and transformers, t, elements, respectively, are calculated from their primitive nodal admittance matrix as function of the nodal voltages applied in each node of their terminals.

d. Capacitors

Capacitors are modeled as constant impedance. Thus, the actual reactive power injected into the network varies with the square of the voltage applied in each node of its terminal.

$$Q^c_\phi = {Q_{nom}}^c_\phi \times \left(V_{\beta^c,\phi}\right)^2 \qquad \forall c\in C, \phi\in\Phi \tag{4}$$

where ${Q_{nom}}^c_\phi$ is the rated power generated by the capacitor c in phase ϕ.

e. Operation Limits:

The magnitude of nodal voltages are constrained to the upper and lower regulatory limits, being able to assume different values depending on the nominal voltage level of the network they are located.

$$\underline{V}_{n,\phi} \le V_{n,\phi} \le \overline{V}_{n,\phi} \qquad \forall n\in N, \phi\in\Phi \tag{5}$$

Lines and transformers loading limits are established in both terminals of these elements.

$$\left(P^l_{①,\phi}\right)^2 + \left(Q^l_{①,\phi}\right)^2 \le \left(V_{\beta^l_{①},\phi} \times \overline{I}^l\right)^2 \quad \forall l\in L, \phi\in\Phi \tag{6}$$

$$\left(P^l_{②,\phi}\right)^2 + \left(Q^l_{②,\phi}\right)^2 \le \left(V_{\beta^l_{②},\phi} \times \overline{I}^l\right)^2 \quad \forall l\in L, \phi\in\Phi \tag{7}$$

$$\left(P^t_{①,\phi}\right)^2 + \left(Q^t_{①,\phi}\right)^2 \le \left(V_{\beta^t_{①},\phi} \times \overline{I}^t\right)^2 \quad \forall t\in T, \phi\in\Phi \tag{8}$$

$$\left(P^t_{②,\phi}\right)^2 + \left(Q^t_{②,\phi}\right)^2 \le \left(V_{\beta^t_{②},\phi} \times \overline{I}^t\right)^2 \quad \forall t\in T, \phi\in\Phi \tag{9}$$

where $\overline{I}^l$ and $\overline{I}^t$ are the ampacities of a line l and transformer t, respectively.

f. Curtailment Limit:

The Brazilian regulation to date allows the connection of DG under the net metering billing mechanism. Thus, it is reasonable to avoid that prosumers are unfairly penalized by being requested to curtail a power greater than their local demand. In the formulation, this is ensured by constraining the generation minimum power to the minimum value between the power available by the solar resource, ${P_{aval}}^g_\phi$, and the local demand of the same CU where the generator g is placed, $P^{u,g}_\phi$ and $P^{u_\delta,g}_\phi$, as shown in equations (10) and (11), to single/three-phase and two-phase CU, respectively.

$$\min\{P^{u,g}_\phi, {P_{aval}}^g_\phi\} \le P^g_\phi \le {P_{aval}}^g_\phi \quad \forall g\in G, \phi\in\Phi \tag{10}$$

$$\min\{P^{u_\delta,g_\delta}, {P_{aval}}^{g_\delta}\} \le P^{g_\delta} \le {P_{aval}}^{g_\delta} \quad \forall g_\delta\in G_\delta \tag{11}$$

According to equations (10) and (11), whenever the power available is less than the local demand, the power generated is equal to the available one.

g. Balanced Generation

For three-phase generators, balanced generation is adopted. This constraint is formulated through the auxiliary variable ${P_{aux}}^g$.

$$P^g_\phi = {P_{aux}}^g \qquad \forall g\in G, \phi\in\Phi | {P_{aval}}^g_\phi \neq 0 \tag{12}$$

It is worth mentioning that the condition ${P_{aval}}^g_\phi \neq 0$ is necessary so that the constraint does not force power injection in nodes that do not exist in single-phase generators.

4. IMPLEMENTATION

The centralized framework of the ANM strategy has been implemented considering specific tools for the emulation of the electrical network and the optimization application, as shown in Figure 2. The network has been modeled in OpenDSS (Dugan and McDermott, 2011), and the formulation presented in section 3 has been modeled through the algebraic modeling language from AIMMS (Bisschop, 2006).

In this software structure there is a clear distinction between network emulation and a component responsible for

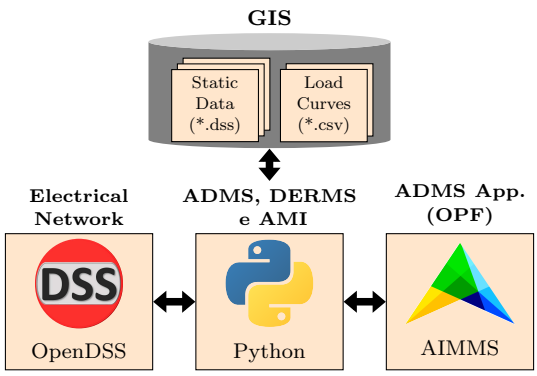

Figure 2. Simulation framework.

representing a corporate system, with access to all network static data, field measurements and other corporate systems.

The core of the simulation framework has been implemented in Python and it is responsible for the network static data reading and loading in both OpenDSS and AIMMS, the control of the simulation, the communication between the two tools, obtaining measurement data from the simulated network and sending optimal commands to each control element.

The timing of the events involved in the simulation is presented in Figure 3. Each mark in the axis corresponds to a simulation time instant t. The time step is Δt. In a given time instant, t_s, all the measures monitored by the SCADA, AMI and DERMS systems are sampled and made available to the ADMS for utilization in the application responsible for executing the optimization. After an interval, Δt_d, that represents the communication delays, the time to run the optimization and to send the optimal actions back to each control element in the field, the calculated optimal actions are effectively executed in the network emulator at t_{action}. The process repeats at every ΔT_{cycle} time interval.

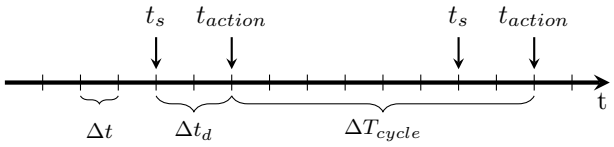

Figure 3. Control cycle and simulation timing.

It is worth to highlight that, in practice, the data monitored in real-time would be continuously sent to the control room, without synchronism. The associated applications (such as the topology processor and the state estimator) would then consider the most recent data of each element and monitored measures. In the same manner, depending on the communication infrastructure utilized and the implementation/settings of the primary controller of each control element, the actions would be executed at slightly different time instants. For instance, different ramp rates might be applied to different DER (IEEE, 2018).

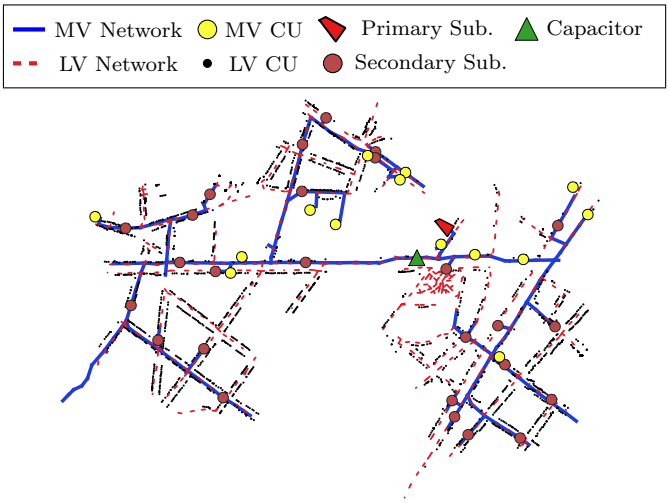

Figure 4. Network topology.

5. CASE STUDY - A BRAZILIAN REAL NETWORK

5.1 Description

The network under study is illustrated in Figure 4. It is located in a Brazilian urban area and comprises a 13.8 kV MV feeder with maximum extension of 1.35 km, 27 127/220 V three-phase LV feeders and 841 kW of peak demand. The network topology, consumer class of each CU and load shapes with hourly granularity, based on measurement campaigns, have been provided by the local utility.

The network modeling in OpenDSS format closely follows the regulation established for the calculation of regulatory technical losses (ANEEL, 2018) which includes, among others, three-phase three-wire modeling, and detailed modeling of the LV feeders, including the service cables and single, two and three-phase CU. The loads have been modeled with 0.92 fixed power factor and a constant power. The model comprises a total of 4915 nodes.

5.2 Random Allocation of PV Systems

To generate a realistic deployment scenario, typical PV installed capacity per customer class and connection has been utilized. For that, data of real DG developers located at the concession area of the local utility have been considered (ANEEL, 2019). By crossing these data with consumer class and connection type of each CU, a PV installed capacity cumulative frequency curve has been set up for two-phase and three-phase residential and three-phase commercial CU, Figure 5. Based on this curve, 5 kWp, 7.5 kWp and 16 kWp of installed capacity were considered for these CU, respectively, which represent around 70% of all CU with PV installed in the concession area for these customer classes and connection types.

This procedure has been adopted since the existence of a few CU with a considerably higher installed capacity would take the simple average to higher and non-realistic values to be considered in this study.

For MV CU, 40 kWp of installed capacity has been adopted based on the average of the only four customers of this class located at the concession area of the local

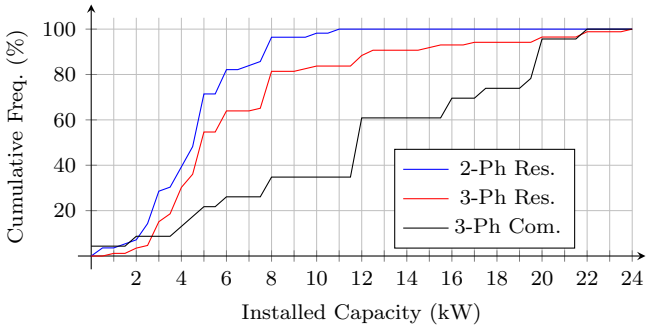

Figure 5. PV installed capacity cumulative frequency in residential and commercial CU.

utility. Due to missing data, 2 kWp of installed capacity has been adopted for single-phase CU, and, for two-phase commercial CU, the same value for residential CU has been assumed, which was 5 kWp of installed capacity.

During the network preparation, the installed capacity per customer and connection type aforementioned data led to extremely severe overvoltages and overloadings even for low penetration values, which could mask the effectiveness of the proposed ANM strategy between control cycles. Furthermore, as one of the objectives is to verify the robustness of the OPF against a large number of control elements, the leveraged installed capacity data have then been scaled down in 50%, i.e., 1 kWp, 2.5 kWp, 3.75 kWp, 8 kWp and 20 kWp have been considered for single-phase (residential and commercial), two-phase (residential and commercial), three-phase residential, three-phase commercial and MV CU, respectively.

As for the connection and phasing of the PVs, it is assumed that each PV has exactly the same characteristics of the CU where it is located. The irradiance curve adopted contains a 1-minute resolution and assumes a clear day. It was set up based on the tool presented in Richardson and Thomson (2013), by using the geographical position of the feeder.

The inverter efficiency curve and the PV module temperature coefficient have been extracted from datasheets of commercial inverters and PV modules available in the Brazilian market. As for the daily PV cell temperature, a typical curve has been adopted, with a maximum temperature of 60°C at 1 pm. It is assumed that the inverter is oversized in 20% of the PV array rated peak power such that there is no generation clipping during maximum generation instants, such that any generation limitation is exclusively due to the curtailment setpoints sent by the ADMS application.

Finally, CU have randomly been selected assuming 50% of penetration (defined here as the relative number of CU with PV), which translates to a total PV installed capacity of nearly 215% of the feeder's peak demand. The random allocation resulted in 788 prosumers distributed over the MV and the 27 LV feeders. An hourly simulation has been performed to verify the existence of violations in the scenario without ANM strategy. Figure 6 shows that there are overvoltages greater than 1.2 pu during the hours of maximum irradiance. The maximum and minimum regulatory limits adopted in the simulation were 1.05 pu and 0.921 pu, respectively. Figures 7 and 8 show that there are also a few lines and transformers heavily overloaded. They also show the presence of reverse power flow in several line segments and in all transformers due to the loading evolution resembling the irradiance curve of a clear sky, adopted in the study. This scenario is considered for testing the proposed ANM strategy.

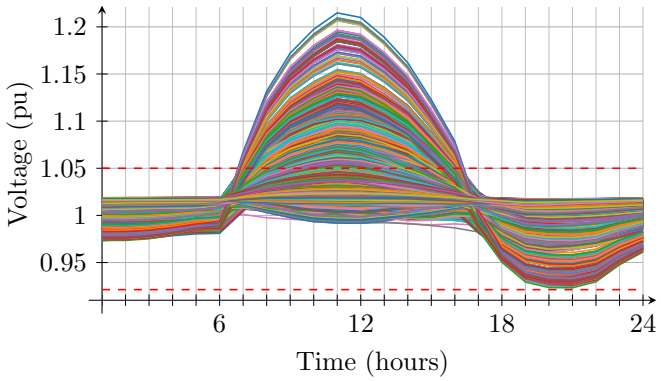

Figure 6. Nodal voltages with PV allocation.

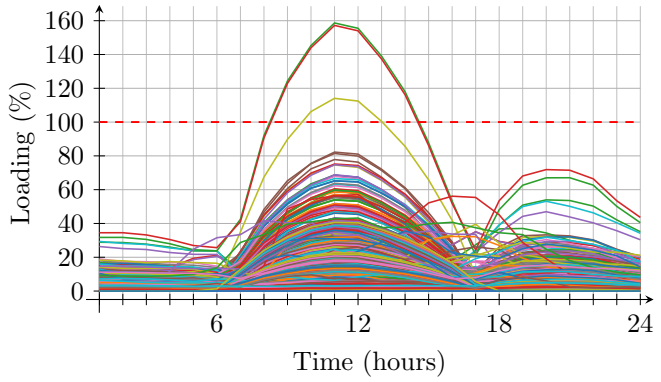

Figure 7. Lines Loading.

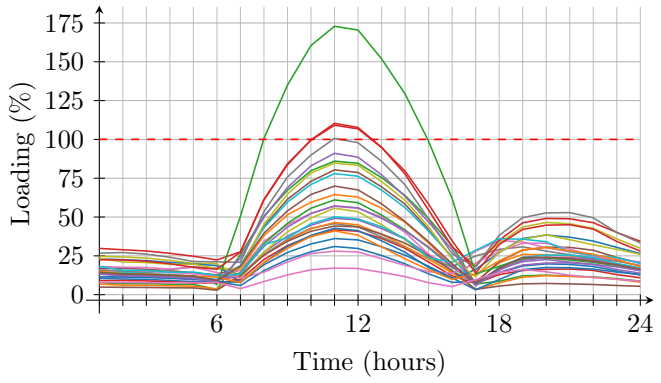

Figure 8. Transformers Loading.

5.3 Formulation Validation

Before executing the ANM strategy, the mathematical formulation presented in section 3 was first validated in a snapshot simulation at the time instant of maximum generation. Considering all nodes of the circuit, the maximum nodal voltage difference between the solution extracted from the optimization engine, AIMMS, and the nodal voltages measured from the network emulator, OpenDSS, after the execution of the optimal curtailment setpoints to each PV system of the network was 5.06×10^{-6} pu

and 1.47×10^{-4} degrees for the magnitude and angle, respectively. These negligible values demonstrate that all constraints of the formulation are satisfied and that the communication between the static data (for instance, impedances of lines and transformers) and dynamic data (such as load demand, curtailment levels) are correctly transferred and translated between OpenDSS and AIMMS through the Python application developed.

It is worth mentioning that during the validation stage, it was verified that the CONOPT 4.0 solver presented the best performance amongst the solvers able to run NL problems available in the academic version of AIMMS. Therefore, it was adopted during the remainder of the study.

5.4 Results

The simulation considering the ANM strategy was performed with a time step Δt of 1 minute, control cycles ΔT_{cycle} of 10 minutes and the optimal actions were executed after a delay Δt_d of 2 minutes. The hourly load shapes were interpolated to fit in the 1-minute simulation time step.

The average optimization execution time was 22.1 seconds, sufficient for the execution in a centralized framework in near real-time and consistent with the time delays adopted.

Network State Figure 9 shows that the ANM strategy was able to limit the nodal voltages between the regulatory limits. However, there was a voltage oscillation around this limit in the morning, with a peak greater than 1.06 pu, from which the oscillations reduced as the instant of maximum irradiance was approached, between 11 am and midday. During this interval, the oscillations were almost inexistent. In the afternoon, they were present until 4 pm, although they happened slightly below the upper regulatory limit.

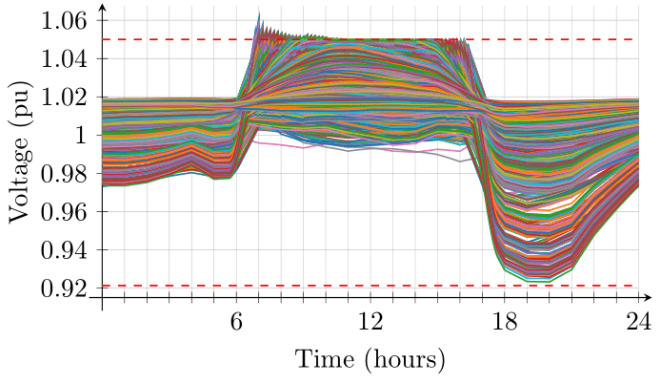

Figure 9. Nodal voltages.

As for the lines loading, Figure 10, all violations were eliminated and the maximum loading was only 80%, which means that the lines loading limit were non-binding constraints of the OPF. This is not true for the transformers loading constraints, since an oscillation with the same characteristics verified for the nodal voltages was also present for two transformers, as highlighted in Figure 11.

The oscillations around the operational limits were related to the timing involved in the ANM strategy. To elucidate this, Figure 11 also highlights the existing oscillations during the morning, between 8:20 am and 9:40 am. Each marker on the curve corresponds to a specific time instant. In each control cycle, there was a leap in the loading, in which it was reduced due to the execution of the optimal curtailment setpoints.

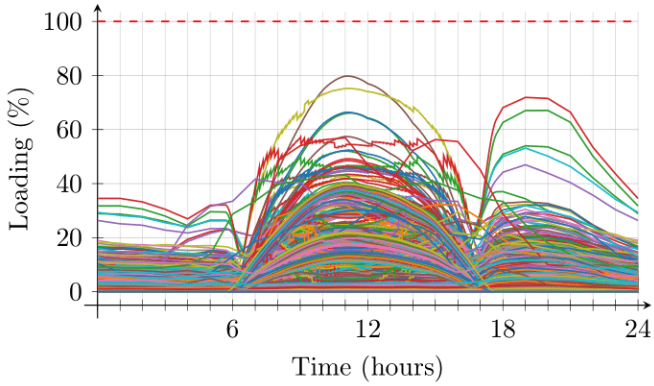

Figure 10. Lines loading.

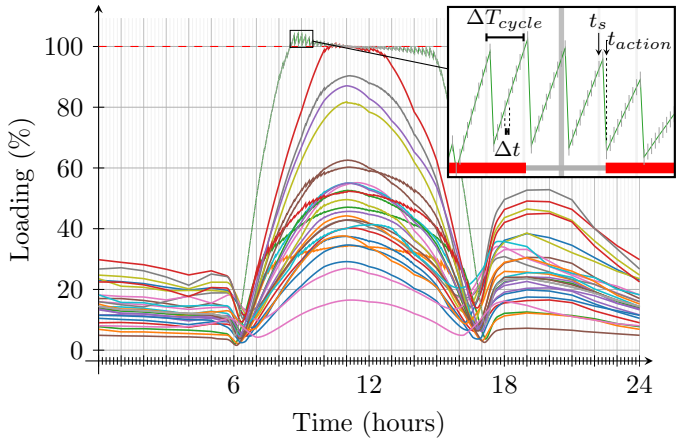

Figure 11. Transformers loading.

During a control cycle, right after the execution of the optimal curtailment setpoints, the loading increased again. This is explained by the fact that, during the morning, the solar irradiance for a clear day is increasing, such that the reverse power flow in the transformers also increases.

One can also note that the slope of the increasing loading reduces. This is due to the derivative of the solar irradiance during the time period analyzed, which is decreasing. The lower the derivative, the lower the increase in the reverse power flow between subsequent control cycles. This also explains why near the maximum irradiance instant the oscillations were practically null.

It is worth highlighting that even after executing the optimal setpoints in each PV system, there were still voltage and loading violations. The reason is due to the communication delay adopted between the sampling and optimal setpoints execution instants. It takes the application of the optimal setpoints to a network state different from which it has been calculated for. During the morning, as the solar irradiance increases, the applied curtailment was lower than the needed at the time instant when they were executed and, by consequence, the violations were not completely avoided. Note that the irradiance derivative has

also influence over how far from the upper limit the loading was at the instant of execution of optimal control actions.

In practice, a simple way to compensate for this inherent delay is to relax the upper limit by lowering and increasing it in the formulation during the morning and the afternoon, respectively. Another option is to utilize a Model Predictive Control (MPC) with estimations for the load demand and PV systems generation in a multi-period optimization. In both cases, the violations are expected to reduce, although at the expense of an increase in the curtailment.

Local Generation and Demand in CU Figure 12 shows the net injected power in the grid as well as the local demand and generation for three selected CU.

In Figure 12a, one can note that there was net injection from 9 am to 2 pm and that the ANM strategy did not request curtailment at any time for this particular CU. In case of Figure 12b, the PV installed capacity is greater than the double of the maximum local demand, which also has a high load factor. Thus, there is net power injection in almost all hours of sun and curtailment during hours of maximum generation, with a peak of 0.6 kW or 24% of the available power, at 11:15 am. The total curtailed energy was 1.8 kWh. Finally, Figure 12c highlights a prosumer in which the maximum curtailment is applied, i. e., the curtailment level that led to a condition in which the local generation supplied entirely and uniquely the local demand, without net power injection into the grid, in accordance to the respective constraints of the mathematical formulation. In this case, the maximum curtailment reached 82% of the available power and the total non-harvested energy was 5.21 kWh.

Curtailment Level Figure 13 shows the total curtailment in the network. One can note that the ADMS sent the first curtailment command at 7 am and it lasted until 4 pm. Again, one can note small variations due to the timing associated with the 10-minute control cycles adopted in the ANM strategy.

As expected, the maximum curtailment was coincident with the maximum PV generation instant, as expected, and it totalized 240 kW, which represents only 12.5% of the total available power. Note that this value is relatively low considering that the total PV installed capacity is about 215 % of the feeder's peak demand, which highlights the strength of the proposed OPF-based ANM strategy. The total energy curtailed throughout the day is 1249 kWh. The total curtailment did not reflect the curtailment applied in each network. In this sense, Figure 14 shows the curtailment to each of the 27 networks that comprise the grid. It can be seen that, in reality, there were networks that had a maximum curtailment as high as 40%. On the other hand, there was significant curtailment in only half of the networks. This can point to DNO which LV networks most need upgrades such as the installation of *On-Load Tap Changer* (OLTC)-fitted secondary transformers.

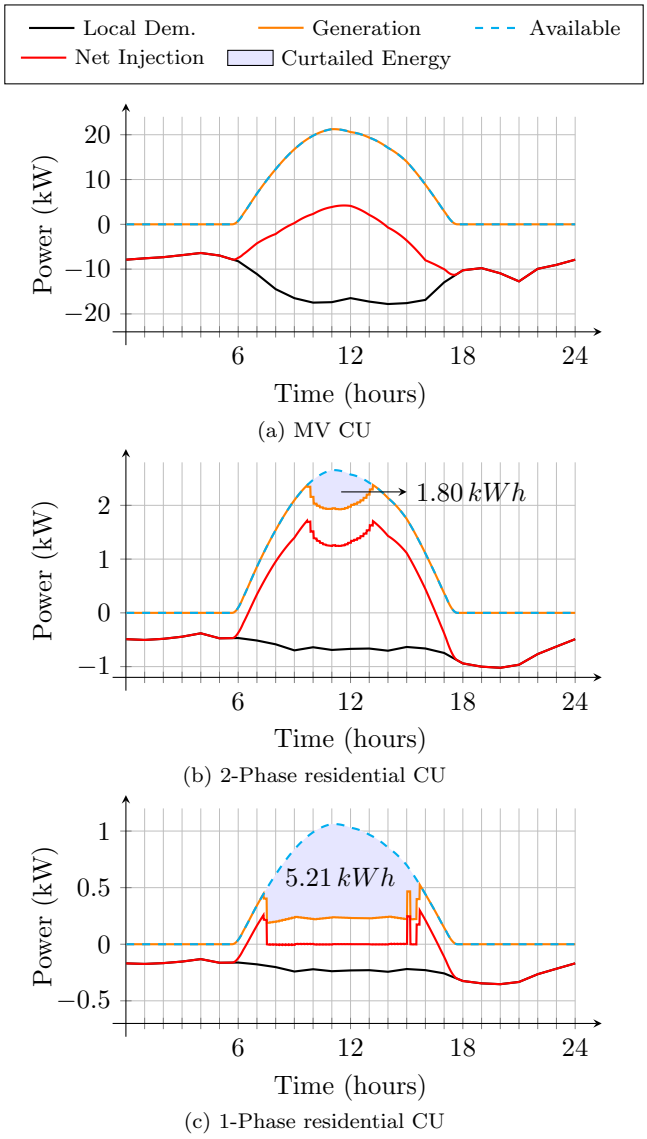

(a) MV CU

(b) 2-Phase residential CU

(c) 1-Phase residential CU

Figure 12. Powers in selected CU.

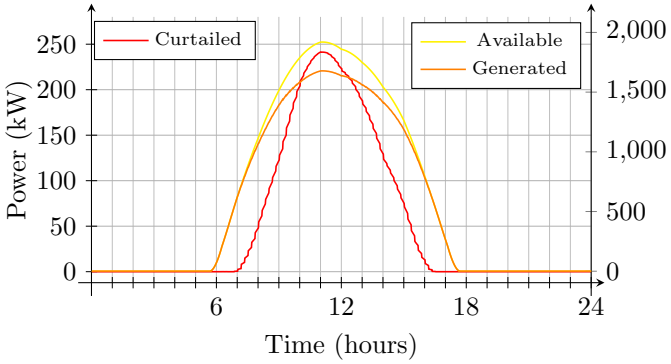

Figure 13. Curtailed, available and generated total powers.

6. DISCUSSION AND CONCLUSIONS

High DER (such as DG) penetration levels require new strategies to operate the distribution networks through a better utilization of all flexibility provided by the available resources. Although centralized ANM strategies based on OPF can perform such task, this type of solution has not been widely adopted yet for several reasons. From the regulatory perspective, new policies are needed to allow flexible interconnection agreements between DNO and the prosumers, allowing that the DG unit, resource acquired and payed by the prosumer, to be, in fact, integrated to the operational processes of the DNO.

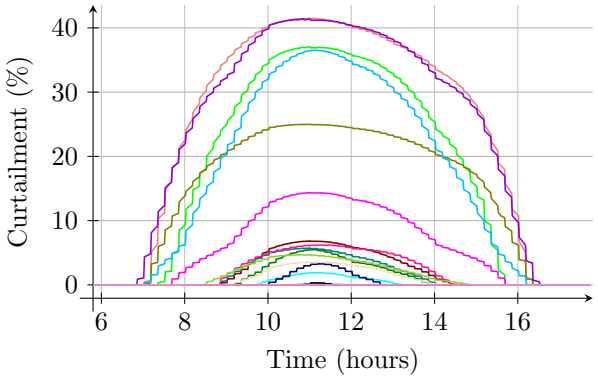

Figure 14. Curtailment per network.

From the economics point of view, one can say that the main barrier is the need to build a communication infrastructure that allows the treatment of a high number of measurements in real-time, providing full visibility of the network, which has a high initial cost. Also, it is necessary that the strategy adopted do not significantly impact the return of investment of the DG developers. As for the curtailment particular case, the definition of a maximum static curtailment or rules for sharing the curtailment between different DG owners placed in the same region/network can be adopted.

This paper presented a centralized ANM strategy based on a NL, three-phase unbalanced OPF formulation that seeks to maximize the energy harvested by PV systems installed across LV and MV feeders while simultaneously mitigating voltage and loading levels violations. A case study analyzed a real Brazilian distribution network with detailed modeling down to the LV customers. A realistic PV deployment scenario with 788 PV systems was considered. The results show that formulation utilized is robust enough to solve problems of real dimensions in a suitable time for the near real-time ANM strategy. It was also verified that the timing involved in practice can reduce the effectiveness of the solution in maintaining adequate voltage and loading operational levels, leading to cyclical violations with severity that depends on the penetration level, the duration of the control cycle adopted and the inherent delays involved in the execution of the optimal control actions, making it necessary to incorporate these aspects in the proposed solution.

REFERENCES

ABNT (2013). Sistemas Fotovoltaicos (FV) - Características da Interface de Conexão com a Rede Elétrica de Distribuição.

ANEEL (2018). Módulo 7 - Cálculo de Perdas na Distribuição.

ANEEL (2019). Geração Distribuída. URL `http://www.aneel.gov.br/geracao-distribuida`.

Argonne National Laboratory (2015a). DMS Functions. Technical report, Argonne Natioal Laboratory.

Argonne National Laboratory (2015b). Requirements for Implementing Advanced Distribution Management Systems. Technical report, Argonne Natioal Laboratory.

Bisschop, J. (2006). *Aimms Optimization Modeling*. Paragon Decision Technology. URL `https://books.google.com.br/books?id=oHR8vSZFMvgC`.

Bruendlinger, R. (2016). Review and Assessment of Latest Grid Code Developments in Europe and Selected International Markets with Respect to High Penetration PV. *6th Solar Integration Workshop*, (December).

Currie, R.S.G.S., Ault, G.S.G.S., Foote, C., and McDonald, J. (2007). Active power-flow management utilising operating margins for the increased connection of distributed generation. *IET Generation, Transmission & Distribution*, 1(1), 197.

Dugan, R.C. and McDermott, T.E. (2011). An open source platform for collaborating on smart grid research. In *2011 IEEE Power and Energy Society General Meeting*, 1–7. IEEE.

Hrnjic, T., Fetic, N., and Husagic-Selman, A. (2017). Data Structures and Implementation of Fast Distribution System Power Flow and State Estimation. In *2017 9th IEEE-GCC Conference and Exhibition (GCCCE)*, 1–9. IEEE.

IEEE (2018). Standard for Interconnection and Interoperability of Distributed Energy Resources with Associated Electric Power Systems Interfaces. *IEEE Std 1547-2018 (Revision of IEEE Std 1547-2003)*, 1–138.

International Energy Agency (IEA) (2019). *Renewables 2019*. Market Report Series: Renewables. OECD.

Richardson, I. and Thomson, M. (2013). Integrated simulation of photovoltaic micro-generation and domestic electricity demand: A one-minute resolution open-source model. *Proceedings of the Institution of Mechanical Engineers, Part A: Journal of Power and Energy*, 227(1), 73–81.

Seal, B.E. and Ealey, B.E. (2016). Common Functions for Smart Inverters: 4th Edition. Technical report, EPRI.

Seal, B.E., Renjit, A.E., and Deaver, B.E. (2018). Understanding DERMS. Technical Report June, EPRI.

Appendix A. 2-PHASE LOADS FORMULATION

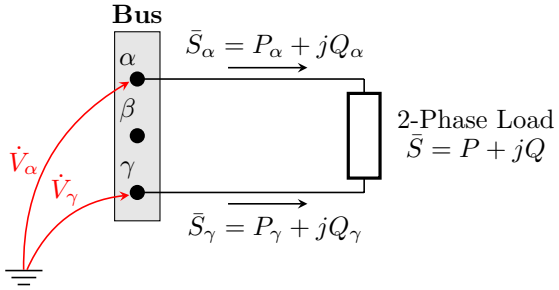

Figure A.1. 2-Phase load connected to nodes α and γ of a bus.

Given the power, $\bar{S}$, consumed by a two-phase load connected to phases α e γ and with nodal voltages $\dot{V}_\alpha = V_\alpha \angle \theta_\alpha$ and $\dot{V}_\gamma = V_\gamma \angle \theta_\gamma$, respectively, the active and reactive power consumed in a phase φ can be written as:

$$P_\varphi = \frac{P\left(V_\varphi\right)^2 - PV_\varphi V_\phi \cos\left(\theta_{\varphi\phi}\right) + QV_\varphi V_\phi \sin\left(\theta_{\varphi\phi}\right)}{\left(V_\varphi\right)^2 + \left(V_\phi\right)^2 - 2V_\varphi V_\phi \cos\left(\theta_{\varphi\phi}\right)} \quad \forall \varphi, \phi \in \{\alpha, \gamma\} \,|\, \phi \neq \varphi \tag{A.1}$$

$$Q_\varphi = \frac{Q\left(V_\varphi\right)^2 - QV_\varphi V_\phi \cos\left(\theta_{\varphi\phi}\right) - PV_\varphi V_\phi \sin\left(\theta_{\varphi\phi}\right)}{\left(V_\varphi\right)^2 + \left(V_\phi\right)^2 - 2V_\varphi V_\phi \cos\left(\theta_{\varphi\phi}\right)} \quad \forall \varphi, \phi \in \{\alpha, \gamma\} \,|\, \phi \neq \varphi \tag{A.2}$$